Available online at www.sciencedirect.com

ScienceDirect

Geochimica et Cosmochimica Acta 151 (2015) 86–102

Geochimica et Cosmochimica Acta

www.elsevier.com/locate/gca

Partitioning of Cu between mafic minerals, Fe–Ti oxides and intermediate to felsic melts

Xingcheng Liu [a,c], Xiaolin Xiong [a,*], Andreas Audétat [b], Yuan Li [b]

[a] State Key Laboratory of Isotope Geochemistry, Chinese Academy of Sciences, Guangzhou 510640, China
[b] Bayerisches Geoinstitut, Universität Bayreuth, D-95440 Bayreuth, Germany
[c] University of the Chinese Academy of Sciences, Beijing 100049, China

Received 21 May 2014; accepted in revised form 9 December 2014; Available online 16 December 2014

Abstract

This study used improved capsule technique i.e., $Pt_{95}Cu_{05}$ or $Au_{95}Cu_{05}$ alloy capsules as Cu sources to determine Cu partitioning between mafic minerals, Fe–Ti oxides and intermediate to felsic melts at 0.5–2.5 GPa, 950–1100 °C and various oxygen fugacities (fO_2). In combination with the data from the mafic composition systems, the results demonstrate that Cu is generally highly incompatible in mafic minerals and moderately incompatible to compatible in Fe–Ti oxides. The general order of mineral/melt Cu partition coefficients (D_{Cu}) is garnet (0.01–0.06) ⩽ olivine (0.04–0.20) ≈ opx (0.04–0.24) ≈ amphibole (0.04–0.20) ⩽ cpx (0.04–0.45) ⩽ magnetite, titanomagnetite and Cr-spinel (0.18–1.83). The variations in D_{Cu} depend mainly on temperature, fO_2 or mineral composition. In general, D_{Cu} for olivine (and perhaps opx) increases with decreasing temperature and increasing fO_2. D_{Cu} increases for cpx with Na^+ (pfu) in cpx, for magnetite and Cr-spinel with Fe^{3+} (pfu) in these phases and for titanomagnetite with Ti^{4+} (pfu) in this phase.

The large number of D_{Cu} data (99 pairs) serves as a foundation for quantitatively understanding the behavior of Cu during magmatic processes. The generation of intermediate to felsic magmas via fractional crystallization or partial melting of mafic rocks (magmas) at deep levels of crust involves removal of or leaving assemblages of mafic minerals + Fe–Ti oxides ± sulfides. With our D_{Cu} data on mafic minerals and Fe–Ti oxides, D_{Cu}^{bulk} values around 0.2 were obtained for the sulfide-free assemblages. Cu will thus be concentrated efficiently in the derived melts during these two processes if sulfides are absent or negligible, explaining that high fO_2 and sulfide-destabilization are favorable to formation of the porphyry Cu system.

1. INTRODUCTION

Understanding the behavior of Cu during magmatic processes aids in understanding crust–mantle differentiation, the formation of magmatic and magmatic-hydrothermal ore deposits, and the redox state of the upper mantle (e.g., Lee et al., 2012; Audétat and Simon, 2013; Li and Audétat, 2013; Li, 2014; Liu et al., 2014). Partition coefficient of Cu (D_{Cu}) between mineral and melt is a key parameter for quantitatively understanding the behavior of Cu. As a strong chalcophile element, the partitioning of Cu between sulfides and silicate melts has been extensively studied (e.g., Jugo et al., 1999; Ripley et al., 2002; Simon et al., 2006, 2008; Bell et al., 2009; Li and Audétat, 2012; Kiseeva and Wood, 2013; Zajacz et al., 2013). However, the partitioning of Cu between silicate minerals, oxides, and silicate melts has received only limited attention (Fellows and Canil, 2012; Lee et al., 2012; Liu et al., 2014). Furthermore, as has been pointed out by Liu et al. (2014), the available Cu partitioning data between silicate minerals, oxides and silicate melts in the literature are inconsistent with each other, with variations of over two

* Corresponding author. Tel.: +86 20 8529 0287.
E-mail address: xiongxl@gig.ac.cn (X. Xiong).

http://dx.doi.org/10.1016/j.gca.2014.12.010
0016-7037/

orders of magnitudes, ranging from 0.02 to 4.1 for olivine, 0.03 to 2.8 for opx, 0.01 to 1.5 for cpx, 0.05 to 5.71 for amphibole, 0.004 to 0.69 for garnet, 0.004 to 1.5 for plagioclase and 0.22 to 26 for Fe–Ti oxides (Table S1). The partitioning data in the old literature obtained by analyzing natural phenocryst/matrix pairs may be elevated artificially owing to the presence of tiny sulfide inclusion in the phenocryst (Lee et al., 2012). On the other hand, most previous D_{Cu} values obtained experimentally also appear to be considerably uncertain because of the problem of alloying between Cu in the sample and the used noble metal capsule. For instance, in the studies of Adam and Green (2006) and Fellows and Canil (2012), continuous Cu-loss from the samples into the noble metal capsules led to extremely low Cu concentration in the silicate melts and thus large analytical uncertainties for Cu, and might also have resulted in disequilibrium partitioning of Cu between the investigated silicate phases.

However, recent experimental studies (Zajacz et al., 2011, 2012, 2013; Liu et al., 2014) demonstrated that the use of Cu-bearing alloy capsules sufficiently resolved the problem of Cu-loss, and that the D_{Cu} values obtained with such capsules are more accurate. Following the study of Liu et al. (2014) who used Cu-bearing Pt capsules to determinate the D_{Cu} values between upper mantle minerals and mafic melts at 1.0–3.5 GPa, 1150–1300 °C and fO_2 of ~FMQ−2 to ~FMQ+5, this study reports Cu partition coefficients between olivine, orthopyroxene, clinopyroxene, amphibole, garnet, plagioclase, Fe–Ti oxides and intermediate to felsic melts, obtained experimentally with Cu-bearing Pt or Au capsules at 0.5–2.5 GPa, 950–1100 °C and fO_2 of ~FMQ−2 to ~FMQ+4.7. The aim is to provide a coherent dataset of Cu partition coefficients that serve as a foundation for quantitatively understanding the behavior of Cu in magmatic processes. To exemplify the potential applications we use these partitioning data to constrain the bulk Cu partition coefficients between sulfide-free assemblages and intermediate to felsic magmas since they are associated with the formation of Cu porphyry deposits (Hou et al., 2011; Richards, 2011; Sun et al., 2013; Loucks, 2014).

2. EXPERIMENTAL AND ANALYTICAL METHODS

2.1. Starting materials

To investigate the Cu partitioning between mafic minerals, Fe–Ti oxides and intermediate to felsic melts, three starting compositions including a MORB, a K-basalt, and a dacite were selected or synthetized (Table 1). The K-basalt is a natural potassic basalt from Chinese Tianshan (Xiong et al., 2005). The MORB is a synthesized basalt compositionally similar to the average N-MORB (Liu et al., 2014). The two basalt compositions will produce minerals + basaltic–andesitic melts in the P–T conditions of this study. The dacite was synthetized from reagent grade oxides and carbonates in the same way as the MORB composition was prepared (Liu et al., 2014). ~100 ppm Rb as rubidium hydroxide was added to these three compositions. To improve their chemical homogeneity, two rounds of melting (1500 °C)–quenching–grinding were performed.

Table 1
Starting compositions (EMPA in wt.%).

	MORB	K-basalt	Dacite
SiO_2	50.07(0.58)	49.28(0.21)	65.74(0.25)
TiO_2	1.66(0.05)	1.68(0.06)	0.49(0.05)
Al_2O_3	15.38(0.15)	16.36(0.14)	16.24(0.13)
FeOt	10.80(0.24)	10.51(0.16)	4.90(0.11)
MnO	0.02(0.01)	0.33(0.03)	0.02(0.02)
MgO	6.80(0.11)	7.27(0.07)	2.19(0.03)
CaO	11.61(0.19)	6.81(0.04)	3.80(0.08)
Na_2O	2.83(0.11)	3.88(0.07)	4.70(0.21)
K_2O	0.23(0.02)	1.37(0.05)	1.51(0.03)
P_2O_5	0.30(0.02)	0.37(0.03)	0.04(0.02)
NiO	0.03(0.01)	0.05(0.01)	0.03(0.03)
Cr_2O_3	0.01(0.01)	0.09 (0.01)	0.05(0.01)
Total	99.74(0.97)	98.01(0.50)	99.69(0.44)

The MORB composition is from Liu et al. (2014). Numbers in parenthesis are analytical uncertainties of 1σ standard deviations (n = 7–10). The total of K-basalt is lower than 99% because this natural sample contains trace elements that were not analyzed by the EMP (e.g., Cl, S, and other trace elements).

Before the last round of grinding in producing sample powders, several aliquots of the quenched glasses were left for analyses with electron microprobe (EMP). The results are presented in Table 1.

2.2. Sample capsules and Cu sources

Except for two dacite runs (marked with asterisk in Table 2) conducted with $Au_{95}Cu_{05}$ alloy capsules with 2.7 mm ID, 3.0 mm OD and 6–8 mm length, all the other runs were performed with $Pt_{95}Cu_{05}$ alloy capsules with the same size. The $Pt_{95}Cu_{05}$ or $Au_{95}Cu_{05}$ capsule also serves as the Cu source of the samples (Cu diffuses from capsule into sample during experiment). 10–15 mg sample powder plus <10 wt.% H_2O was loaded into each capsule (~5 wt.% H_2O for MORB and K-basalt samples and ~10 wt.% H_2O for dacite samples). With P = 0.5–2.5 GPa in this study, the H_2O added will not result in water saturation in the melts based on the H_2O solubility of silicate melt at $P \geqslant 0.5$ GPa (e.g., Holtz et al., 2001). All the sample capsules were crimped and welded shut using the precision welding machine of LAMPERT PUK U3 and were weighed before and after welding to ensure no leakage. The single $Pt_{95}Cu_{05}$ or $Au_{95}Cu_{05}$ capsule is 180–250 mg before sample is filled, which is over 10 times higher than the mass of sample plus H_2O. The Cu content of each phase during an experiment thus would be buffered to a constant by the $Pt_{95}Cu_{05}$ or $Au_{95}Cu_{05}$ capsule. The supplementary material SMT1 demonstrated that moderate Fe-gain from the samples or buffer materials does not cause a significant change of the Cu content in the capsules; only in the case with NNO buffer materials in the double-capsule setups, Cu contents at the inner rims of capsules show slight to moderate decline (10–47% relative) due to Cu diffusion and loss into the buffer materials and simultaneously significant Ni + Fe gain from the sample and buffer materials. Even in this case, Cu content of each phase

Table 2
Experimental conditions and results.

Sample a[a]	Run No.[b]	H_2O Initial	fO_2 [c] buffer	P (GPa)	T (°C)	Time (h)	Products (phase assemblages)[d]	[e]Xnf/X	Cu[f] in melt	Fe[g] loss	fO_2[h] ΔFMQ
Starting material: MORB											
M-1	HG-LG-b#	6.0%	NNO	1.5	1050	108	gl(89), cpx(11)	0.59	275	78%	
M-2	Cu-22#	4.9%	–	1.0	1100	77	gl(88), cpx(10), mag(2)	0.55	2564	3%	
M-3	Cu-28#	4.9%	–	1.0	1070	78	gl(68), cpx(28), mag(2), Ti-mag(3)	0.61	1448	21%	
M-4	HGG3-b#	5.2%	NNO	1.0	1000	112	gl(89), cpx(11)	0.58	650	70%	>+0.8
M-5	XT168N-4a#	6.8%	HM	1.0	950	156	gl(61), amp(11), cpx(21), Ti-mag(8)	0.61	1651	0%	
M-6	XT168N-7b#	5.5%	NNO	0.5	1000	88	gl(88), cpx(8), mag (1), Ti-mag(3)	0.56	8740	3%	+4.7
M-7	XT168N-8b#	4.9%	HM	0.5	1000	88	gl(81), cpx(12), mag (3), Ti-mag(4)	0.58	2465	3%	+3.0
Starting material: K-basalt											
K-1	XT168N-2a#	4.6%	NNO	2.0	1000	91	gl(66), cpx(1), amp(24), grt(9)	0.64	191	59%	>−1.6
K-2	XT168N-3#	6.2%	HM	2.0	1000	94	gl(75), amp(17), mag (5), Ti-mag(2)	0.60	1983	0%	+1.6
K-3	XT168N-6a#	5.7%	WM	2.0	1000	100	gl(90), ol(2), amp(5), mag(4)	0.59	1471	16%	+1.2
K-4	XT168N-1b#	5.9%	NNO	1.0	950	145	gl(78), amp(20), mag(2)	0.61	444	36%	
K-5	XT168N-4b#	5.5%	HM	1.0	950	156	gl(60), amp(32), mag (4), Ti-mag(4)	0.67	988	0%	
K-6	XT168N-7a#	5.4%	NNO	0.5	1000	88	gl(89), ol(2), mag (6), Ti-mag(3)	0.60	7123	0%	+4.4
K-7	XT168N-8a#	5.1%	HM	0.5	1000	88	gl(89), ol(3), mag(8)	0.60	2020	2%	+2.7
K-8Ti	XT168N-Ti#	5.1%	-	2.0	990	100	gl(50),amp(24),grt(15),cpx(8),Ti-mag(3), Cr-spl(trace)	0.69	604	5%	+0.1
Starting material: Dacite											
D-1	Dacite-L4	9.7%	FMQ	2.5	975	123	gl(87), grt(12), sillimanite (1)	0.77	511	11%	
D-2	Dacite-L11	6%	NNO	2.0	1000	80	gl(95), cpx(4), opx(1), Cr-spl(trace)	0.74	222	54%	>−1.4
D-3	Dacite-L17	9.2%	NNO	2.0	1000	159	gl(94), grt(2), cpx(3), Ti-mag(1)	0.75	797	19%	+0.4
D-4	Dacite-L2	9.9%	NNO	2.0	1000	96	gl(95),cpx(4), grt(1)	0.74	72	91%	>−2.9
D-5	Dacite-L6	9.9%	HM	2.0	1000	95	gl(98), grt(1), cpx(1)	0.73	210	65%	>−1.5
D-6	Dacite-L7	9%	FMQ	2.0	1000	192	gl(98), cpx(2)	0.73	103	98%	>−2.4
D-7	Dacite-L9	9.3%	Graphite	2.0	1000	88	gl(96), grt(3), cpx(1), Cr-spl(trace)	0.74	452	36%	⩾−0.4
D-8*	Dacite-L14	10%	Graphite†	1.0	950	119	gl(60),opx(8),cpx(5),pl(26),Ti-mag(1),ilm(1)	0.80	112	0%	−0.3
D-9	Dacite-L15	10.9%	HM	1.0	950	154	gl(95), amp(3), Ti-mag(2)	0.74	480	20%	
D-10	Dacite-L16	9.2%	NNO	1.0	950	170	gl(95), amp(4), cpx(1)	0.74	52	93%	
D-11*	Dacite-L19	8.9%	FMQ	1.0	950	163	gl(90), amp(10)	0.76	17	25%	
D-14Ti	Dacite-Ti#	9.9%	–	2.0	990	100	gl(95), cpx(3), Ti-mag(1), rut(1)	0.72	689	33%	⩾+0.3

[a] Single capsule ($Pt_{95}Cu_{05}$) runs include M-2, M-3, K-8Ti and D-14Ti; other runs are double-capsule runs with outer Pt capsule and inner $Pt_{95}Cu_{05}$ capsule or $Au_{95}Cu_{05}$ capsule (marked with asterisk *).

[b] Run No. marked with # were performed at Guangzhou; the other runs were performed at Bayreuth.

[c] fO_2 buffer in the double-capsule runs. Graphite† (D-8) is a run conducted with a graphite-lined $Pt_{95}Cu_{05}$ capsule with no lids at the two ends of the graphite cylinder. "–" means "no buffer" in the single runs.

[d] gl = glass, ol = olivine, opx = orthopyroxene, cpx = clinopyroxene, amp = amphibole, grt = garnet, pl = plagioclase, mag = magnetite, Ti-mag = titanomagnetite, Cr-spl = Cr-spinel, rut = rutile, ilm = ilmenite; Phase proportions calculated by mass balance using EMP data.

[e] X_{nf}/X: Melt polymerization (the sum of the molar fractions of network-forming cations normalized to the sum of the molar fractions of all the cations in the melt), data from Tables S2.

[f] Cu in melt (ppm): apparent Cu solubility buffered by the Cu-bearing capsules, data from Tables S2.

[g] FeO loss relative expressed as 100* (FeO_{calc}–$FeO_{starting\ glass}$)/$FeO_{starting\ glass}$ with FeO_{calc} from mass balance calculation.

[h] The actual fO_2 values at P and T. Runs K-3, K-6 and K-7: calculated from the olivine–spinel equilibrium oxygen barometer of Ballhaus et al. (1991, ±0.4 log units uncertainties above FMQ); run D-8: calculated with the magnetite–ilmenite oxygen barometer of Lepage (2003); other runs at 1000 °C: calculated with the formula log Cu (ppm in melt) = $0.32\log fO_2 + 5.87$ (see text for the details; the values calculated with this model for the runs with severe Fe-loss were shown only for reference).

and Cu partitioning in the sample are considered to be approximately buffered by the Cu-lowered capsule.

2.3. Oxygen fugacity control

Four runs (M-2, M-3, K-8Ti, and D-14Ti in Table 2) were conducted with single $Pt_{95}Cu_{05}$ capsule. The fO_2 for these runs were controlled by the initial oxidation states of the charges (such as Fe^{3+}/Fe^{2+} ratio and H_2O contents) and by the fH_2 imposed by the piston cylinder assemblies. Such a single-capsule setup results in sample fO_2 generally higher than FMQ+1 (Pichavant et al., 2002; Prouteau and Scaillet, 2013; Liu et al., 2014). One run (D-8) was conducted with a graphite-lined $Au_{95}Cu_{05}$ capsule with no lid at the top of the graphite capsule. The sample in this capsule contacted directly the graphite and also the alloy capsule, and the sample fO_2 was controlled/influenced by the graphite. 22 other runs were performed using double capsules and five conventional oxygen buffers [graphite, wüstite–magnetite (WM), fayalite–magnetite–quartz (FMQ), Ni–NiO (NNO), and hematite–magnetite (HM)] in order to impose different levels of fO_2 on the samples. In these double-capsule setups, a sealed sample capsule ($Pt_{95}Cu_{05}$ or $Au_{95}Cu_{05}$) was welded into an outer pure Pt capsule (4.7 mm ID, 5.0 mm OD and 10 mm length). The space between them was filled with buffer materials + H_2O. During a double-capsule run, the fO_2 attained in sample should be lower than the outer theoretical buffer value if the oxygen buffer survived as the sample was always water undersaturated. However, as will be discussed in Section 3.3, only a few runs have been controlled in fO_2 by the buffer assemblages. In most of the runs the actual fO_2 in sample was not controlled by the buffers since they did not last to the end of the experiment.

2.4. Equipment and run procedure

Experiments were conducted at 0.5–2.5 GPa and 950–1100 °C (mostly 950–1000 °C, Table 2) in an end-loaded, solid media piston cylinder, using graphite furnace and half inch diameter $BaCO_3$ assemblies at the Guangzhou Institute of Geochemistry (16 runs) or Talc + Pyrex assemblies at the Bayerisches Geoinstitut (11 runs). The hot piston-in technique was used to pressurize the assembly, and the pressure was regulated automatically during the experiments. Pressure corrections of +13% for the Guangzhou assemblies and +18% for the Bayreuth assemblies were applied, and the pressure uncertainty is believed to be within ±0.1 GPa. Temperatures were measured and controlled using $Pt–Pt_{90}Rh_{10}$ (S-type) thermocouples and were controlled to within ±2 °C of the set-points using a Eurotherm controller. No pressure correction was applied to the thermocouple readings. Temperature uncertainty is believed to be better than ±15 °C by considering a temperature gradient over the capsule. The experiments lasted 77–192 h and then were quenched quickly by switching off the electrical power to the furnace. After each experiment, the recovered capsule was sectioned, mounted in epoxy and polished for optical observations and chemical analyses.

2.5. Analytical techniques

Phase assemblages were identified by optical microscope and EMP. Phase compositions were determined with EMP and LA-ICP-MS.

Oxides (wt.%) of major elements and Cu in minerals and quenched melts were measured with the JEOL JXA-8230 electron microprobe at the Shandong Analysis Center of China Metallurgical Geology Bureau and the JEOL JXA-8200 microprobe at Bayerisches Geoinstitut. Silicate minerals were used as the standards for Si, Ti, Al, Fe, Mn, Mg, Ca, Na, K and P, and metals for Ni, Cr and Cu. The following conditions were applied for the measurements. Beam diameters of 1 μm and 20 μm were used for minerals and quenched melts, respectively. The accelerating voltage was 15 kV at current of 20 nA for all the elements in minerals, and at 20 nA for Cu and 10 nA for other elements in quenched melts. The peak counting time was 10 s for Na and K, 40 s for Cu, and 20 s for the other elements. Analytical errors are: <2% relative for SiO_2, Al_2O_3, and CaO, <3% for FeO, MgO, and TiO_2, and <5% for MnO, Na_2O, and K_2O. Analytical results revealed some Na-loss during analyses of the quenched melts. Mass-balance calculations were performed on all major oxides except for MnO, NiO, Cr_2O_3, CuO and H_2O to estimate the proportions of coexisting phases in a charge and to quantitatively evaluate the charge Fe-loss (see below) during experiment and the melt Na-loss during analysis. The reported Na_2O contents (Table S2) are the corrected values based on the mass-balance calculations.

With the EMP conditions stated above for CuO, we found, by comparison with the results of LA-ICP-MS analyses (Fig. 1), that the EMP data were satisfactory only when CuO content was higher than ~0.05 wt.% (400 ppm

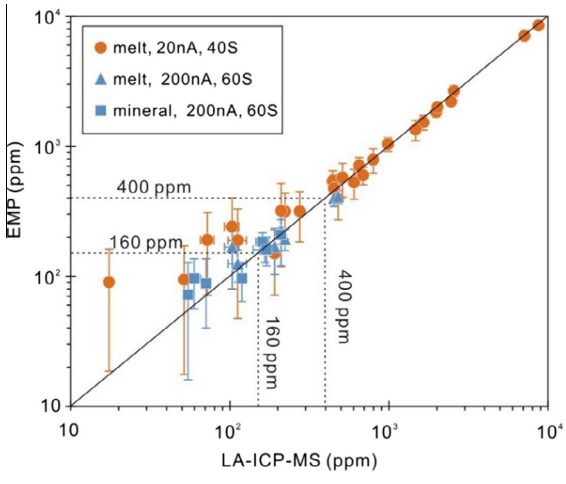

Fig. 1. Comparison of Cu contents determined by EMP and LA-ICP-MS, showing that both methods give identical values within errors when Cu ⩾400 ppm and EMPA with conditions of 15 kV, 20 nA and 40s on the peak and when Cu ⩾160 ppm and EMPA with conditions of 15 kV, 200 nA and 60 s on the peak (see Tables S2–S7, CuO in wt% from the EMP analyses has been converted to Cu in ppm in this figure). Error bars (1σ) depicted only when larger than symbols.

Cu). Therefore, for most of the minerals and melts that returned CuO <0.05 wt.% with conditions of 15 kV, 20 nA and 40 s on peak counting, we re-determined their CuO contents with the conditions of 15 kV, 200 nA and 60 s on peak counting (see Tables S2–S7). At these conditions the calculated detection limit from counting statistics was ~22 ppm CuO and the EMP data appear trustworthy when CuO ⩾ ~0.020 wt.% (160 ppm Cu).

The concentrations of Cu, Rb and Cs (ppm) in quenched melts and in large minerals were determined using the LA-ICP-MS at Guangzhou Institute of Geochemistry or at Bayerisches Geoinstitut. The former uses a Resonetic 193 nm ArF excimer laser attached to an Agilent 7500a ICP-MS; the latter uses a Geolas Pro 193 nm ArF excimer laser attached to an Elan DRC-e ICP-MS. Analytical spots for quenched melts were positioned in the clean areas and those for minerals were positioned in the clean rims. ^{65}Cu, ^{85}Rb and ^{133}Cs were the analyzed isotopes for Cu, Rb and Cs, and the major elements ^{23}Na, ^{25}Mg, ^{28}Si, ^{27}Al, ^{39}K, ^{43}Ca, ^{49}Ti, ^{55}Mn and ^{57}Fe were also analyzed. Detailed operation conditions of the laser are the same as in Liu et al. (2014). An exception is the spot sizes, which in this study were mostly 20–33 μm for mineral and melts, but 15–20 μm and 10–15 μm were also applied in the analyses of relatively small cpxs and amphiboles produced in several dacite experiments (Tables S4 and S5). NIST SRM 610 glass was used as the external standard and Si (or Ca) determined by electron microprobe was used as the internal standard. The reproducibility (1σ) of the measured Cu, Rb and Cs in the SRM 610 standard is <10% relative. We are confident that the Cu minimum detection limits for crystals and quenched melts were better than 0.1 ppm for 20 μm spot and better than 1 ppm for 10 μm spot. The reliability of Cu analyses for minerals was monitored by the time-resolved LA-ICP-MS signals of Rb and/or Cs. Rb and Cs are strongly incompatible in the analyzed minerals and thus contaminations from melt inclusions can easily be recognized by means of elevated Rb and/or Cs signals. The time-resolved LA-ICP-MS signals of Cu revealed that Cu was homogenously distributed in the silicate phases and the analysis was not compromised by any contamination from melt inclusions, tiny accessory minerals or Cu-bearing nuggets.

3. EXPERIMENTAL RESULTS

3.1. Run products

A total of 27 experiments were performed, seven with the starting MORB composition, eight with the K-basalt and twelve with the dacite. These experiments have produced target mafic minerals, Fe–Ti oxides, and intermediate to felsic melts. The experimental conditions and run products are summarized in Table 2.

The MORB runs were conducted at 0.5–1.5 GPa and 950–1100 °C. The 1.5 GPa run (M-1) only produced cpx, and the 1.0 and 0.5 GPa runs produced cpx ± magnetite ± titanomagnetite with amphibole present only in the 950 °C run (M-5). The K-basalt runs were performed at 0.5–2.0 GPa and 950–1000 °C. The 2.0 GPa runs produced amphibole ± garnet ± cpx ± olivine ± magnetite ± titanomagnetite; the 1.0 GPa runs produced amphibole ± magnetite ± titanomagnetite; and the 0.5 GPa runs produced olivine ± magnetite ± titanomagnetite. The dacite runs were conducted at 1.0–2.5 GPa and 950–1000 °C. The 2.5 GPa run produced garnet + sillimanite; the 2.0 GPa runs produced garnet ± cpx ± opx ± spinel ± Ti-magnetite ± rutile; and the 1.0 GPa runs produced amphibole ± opx ± cpx ± titanomagnetite with ilmenite and plagioclase present only in run D-8.

Minerals in most of the runs are euhedral to subhedral (Fig. 2). Mass-balance calculations show that mineral proportions in the sample charge are 2–50% (Table 2). The differences in phase assemblages among the runs that have the same starting material and P–T conditions are ascribed to their difference in H_2O content, fO_2 and/or Fe-loss. In each run, at least one silicate mineral had crystals large enough (usually >20 μm) for LA-ICP-MS analysis, but Fe–Ti oxides, if present, were generally smaller than 10 μm and thus could only be analyzed by EMP. All runs except for run M-3 produced clear melt pools large enough for LA-ICP-MS analysis.

3.2. Melt compositions, Cu solubility and valance

3.2.1. Melt compositions

All the quenched melts are clear with no fluid bubbles found inside the glasses. Their compositions are reported in Table S2 on the anhydrous basis (EMP analyses normalized to 100% anhydrous). The 'by-difference' estimates show that the amounts of dissolved water range from 5.2 to 13.9 wt.%, mainly depending on the initial H_2O contents and the crystallizing amounts. Compared to published melt H_2O solubility data (e.g., Holtz et al., 2001), the 5.2 to 13.9 wt.% H_2O cannot result in H_2O saturation in melts in our run conditions. Therefore, there should be no excess fluid present during the experiments. This is confirmed by the results of optical observations. Melt compositions are mainly controlled by the starting composition and the compositions of the crystallizing phases and their proportions.

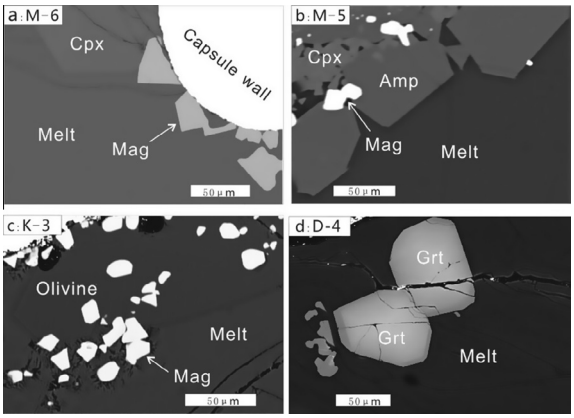

Fig. 2. Representative run products (experimental conditions in Table 2) showing that quenched melts are clean, olivine, clinopyroxene (Cpx), amphibole (Amp) and garnet (Grt) are euhedral and magnetite (Mag) is subhedral.

For the MORB and K-basalt runs, the melt compositions (SiO_2 >~53 wt.% but <63 wt.%) are basaltic–andesitic to andesitic with Mg# ranging mostly from 50 to 65, which are comparable to those of normal basaltic–andesitic rocks. Exceptions are runs M-1, M-4 and K-1. The melts in these runs have relatively high Mg# (80, 73 and 72, respectively, Table S2) due to significant Fe-loss. There are no significant differences in major oxides between the MORB-derived melts and the K-basalt-derived melts except for K_2O, which is five times higher in the K-basalt derived melts (1.52–2.05 wt.% K_2O) than in the MORB derived melts (0.24–0.35 wt.% K_2O). For the dacite runs, the melt compositions (~67–72 wt.% SiO_2) are dacitic to rhyolitic. They are also comparable to those of normal dacites and rhyolites except for generally a bit lower FeO due to different extents of Fe-loss. But the melts from three dacite runs (D-4, D-6 and D-10) experienced severe Fe-loss (>90%), leading to extremely high Mg# (95, 98 and 94, respectively). Melt polymerization degree is expressed as X_{nf}/X, which is defined as the sum of the molar fractions of network-forming cations (i.e., Si and the fraction of Al that can be balanced by Na and K; Nielsen, 1990) normalized to the sum of the molar fractions of all the cations in the melt. The X_{nf}/X values of all the melts are given in Tables 2 and S2.

3.2.2. Cu solubility and valance

Cu contents of the melts range from 275 to 8740 ppm in the MORB derived melts, from 191 to 7123 ppm in the K-basalt derived melts and from 17 to 797 ppm in the dacite derived melts (Tables 2 and S2). Cu contents of the melts from runs with <20% Fe-loss can be approximately taken as the apparent Cu solubility values buffered by the $Pt_{95}Cu_{05}$ or $Au_{95}Cu_{05}$ capsule, since the EMP analyses of capsules confirmed that Cu contents at the inner rims of capsules for the runs without significant Fe-loss are homogeneously close to the capsule initial Cu of 5.76 wt.% (see SMT1). Cu (ppm) in melt vs. X_{nf}/X (melt polymerization) for samples with <~20% Fe-loss from runs with the $Pt_{95}Cu_{05}$ capsules were plotted in Fig. 3a, together with the data from the experiments of Liu et al. (2014) with MORB compositions and the same $Pt_{95}Cu_{05}$ capsules [The komatiite data of Liu et al. (2014) were not used here because the experiments were conducted at 1250–1300 °C]. This figure shows that for a given series of melts (basaltic–andesitic or dacitic melts) or at a given X_{nf}/X value, Cu solubility shows an variation by over one order of magnitude, indicating significant effects of factors such as temperature and fO_2 (see below). This figure also shows that Cu solubility seems to decrease in general from basaltic–andesitic melts to dacitic melts. However, since no Cu solubility data with an identical P–T–fO_2 condition but different melt compositions is available for comparison, it is hard to know if melt composition has an effect with the present data.

In order to test whether or not melt composition has an effect on Cu solubility, we have conducted an additional Cu solubility experiment with three capsules at conditions of 1.5 GPa, 1250 °C and NNO buffer (see SMT2 for the details). In the three-capsule setup, two small $Pt_{95}Cu_{05}$ capsules filled with the MORB sample + H_2O and dacite sample + H_2O, respectively, were welded into a larger Pt capsule. The space between these capsules was filled with NNO buffer + H_2O. Analytical results on the run products show that the MORB and dacite glasses have Cu contents of 5820 ± 131 ppm and 4912 ± 61 ppm, respectively, indicating that the former has 16% higher Cu solubility than the latter at the same P–T and very close fO_2 conditions. This difference would disappear if the slightly higher H_2O (and thus slightly higher fO_2) in the MORB sample is considered (see SMT2). This suggests that melt composition from basaltic to dacitic melts only has a very slight, if any, effect on the Cu solubility. This is actually consistent with the recent results of Zajacz et al. (2013), whose study shows that Cu solubilities in the melts of sulfur-free basalt, andesite and dacite are identical within errors.

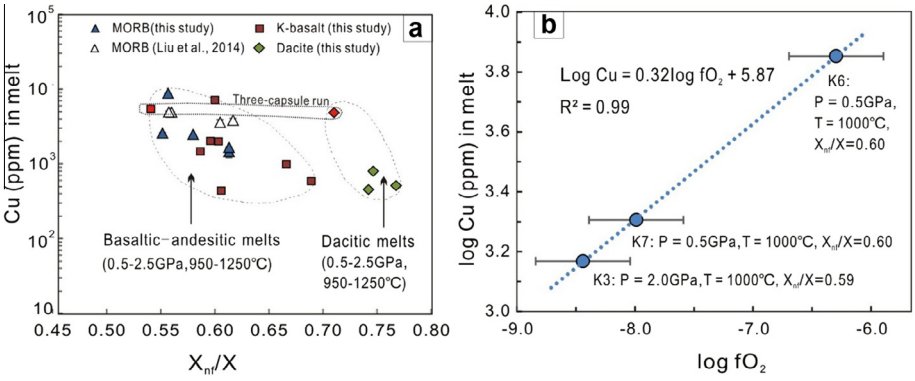

Fig. 3. Cu (ppm) in melt vs. X_{nf}/X (melt polymerization) (a) and log Cu (ppm) in melt vs. fO_2 (b), showing that (a) melt Cu solubility does not vary clearly with melt polymerization, if any, it very slightly decreases with increasing melt polymerization; (b) melt Cu solubility linearly increases with increasing fO_2 and the slope of 0.32 for this straight line indicates that Cu^{1+} was dominant in the melts (see text for the details). The data in (a) are from Table 2 for the runs with $Pt_{95}Cu_{05}$ capsules (data for the runs with > 50% Fe-loss are excluded), also shown for comparison with the data from the experiments of Liu et al. (2014) with the MORB starting materials and the same $Pt_{95}Cu_{05}$ capsules (data for the runs with > 50% Fe-loss are also excluded). The two data points filled with red color in (a) are from the three-capsule run conducted at 1.5 GPa, 1250 °C and the same fO_2 condition (see text and supplementary material SMT2 for the details). The data in (b) are from the runs K-3, K-6 and K-7 in Table 2. (For interpretation of the references to colour in this figure legend, the reader is referred to the web version of this article.)

Previous studies show that melt Cu solubility would not depend on pressure, but dramatically increases with increasing temperature (Holzheid and Lodders, 2001; Zajacz et al., 2013; Liu et al., 2014) and increasing fO_2 (Ripley and Brophy, 1995; Holzheid and Lodders, 2001; Liu et al., 2014). For this study, the effect of fO_2 can be clearly seen from the Cu solubility data from three runs (K-3, K-6 and K-7, Table 2) that had different olivine–spinel equilibrium fO_2 values but nearly same other conditions [$T = 1000$ °C, melt composition $X_{nf}/X = 0.59$–0.60 and Cu contents (wt.%) at the capsule inner rims: 4.88 ± 0.28 for K-3, 5.17 ± 0.14 for K-6 and 5.31 ± 0.16 for K-7]. As shown in Fig. 3b, melt Cu solubility in these runs linearly increases with increasing fO_2. The valence state of dissolved Cu can be estimated using the reaction (Ripley and Brophy, 1995): $Cu^{metal} + n/2\ O_2 = CuO_n^{melt}$, where $\log$Cu solubility (ppm) $= n/2\ \log fO_2 + \log C$. The value of n can be determined from a plot of $\log$Cu (ppm) vs. $\log fO_2$, and a slope of 0.5 ($n = 1$) corresponds to a valence state of 2+, whereas a slope of 0.25 ($n = 0.5$) corresponds to a valence state of 1+. The data from runs K-3, K-6 and K-7 yield a slope of 0.32 ($\log Cu = 0.32 \log fO_2 + 5.87$, Fig. 3b) and a Cu valence state of 1.28 was obtained. This suggests that monovalent Cu (Cu^{1+}) was dominant in the andesitic melts.

3.3. Actual fO_2 of the samples

Actual fO_2 values of the samples in four runs (D-8, K-3, K-6 and K-7) were calculated with the mineral equilibrium oxygen barometers. Run D-8 contains magnetite and ilmenite. fO_2 value in this run is FMQ−0.3 (Table 2) calculated from the magnetite–ilmenite oxygen barometer of Lepage (2003). Runs K-3, K-6 and K-7 were saturated with olivine and Al- and Mg-bearing magnetite (magnetite–spinel solid solution, see Section 3.5.7). fO_2 values for these runs were calculated using the olivine–spinel oxygen barometer of Ballhaus et al. (1991). This oxygen barometer is applicable to the entire spectrum of spinel compositions and gives reasonable results to temperatures as low as 800 °C (Ballhaus et al., 1991). With this oxygen barometer, the calculated fO_2 values for K-3, K-6 and K-7 are FMQ+1.2, FMQ+4.4 and FMQ+2.7 (Table 2), respectively.

In several HM-buffered runs (such as M-7 and K-7) the fO_2 of the samples were lower than their theoretical buffer values and these fO_2 were likely controlled by the buffer. In contrast, actual fO_2 values in runs K-3 (FMQ+1.2) and K-6 (FMQ+4.4) are much higher than their theoretical buffer values (WM and NNO, respectively). Optical observations and EMP analysis indicate that wüstite in run K-3 was exhausted, explaining the buffer failure in this run, whereas Ni and NiO in run K-6 still coexisted but the amount of NiO was clearly increased. We explain that Ni was oxidized and the new produced NiO covered on the surface of the residual Ni and thus led to invalid for the NNO buffer in this run. Scaillet et al. (1992) have demonstrated that most oxygen buffers cannot last for long durations at high temperatures (>700 °C) because the fH_2 imposed by the high-pressure cell assemblage is usually in strong contrast to that of the buffer. The long durations and high temperatures in this study (77–192 h and ⩾950 °C) have caused the buffers in most of the runs being exhausted or invalid as in the cases of runs K-3 or K-6. Their final fO_2 values were controlled by the pressure assembly and the experimental charge.

Cu solubility can provide additional information on actual fO_2 values of the samples because Cu solubility in the sulfur-free systems at a given T, P and melt composition must depend only on fO_2. Assuming the effects of the variations in pressure and melt composition on Cu solubility are negligible, then the fO_2 values in the runs at 1000 °C can be approximately estimated with the formula $\log$Cu (ppm in melt) $= 0.32 \log fO_2 + 5.87$, which is derived from the data of runs K-3, K-6 and K-7 at 1000 °C (see Section 3.2.2 and Fig. 3b for the details). With this formula and Cu solubility data, we have estimated the fO_2 values for the runs at 1000 °C (Table 2). Note that the values obtained by this model for the runs with severe Fe-loss would have moderate to high uncertainties. This is because Cu solubility would be lower compared to the solubility buffered by the $Pt_{95}Cu_{05}$ capsule if Fe-gain and Cu-loss had resulted in a considerable decrease in Cu activity of the capsule (see SMT1). Also because of the same reason, the fO_2 values obtained by this model for the runs with severe Fe-loss would be underestimated, therefore, in Table 2 we experientially use " ⩾ " to imply the actual value close to and " > " to imply the actual value higher than the calculated value. The results in Table 2 indicate that the K-basalt and MORB runs cover a fO_2 range from >FMQ−1.6 to FMQ+4.7, whereas the dacite runs have fO_2 in the range from >FMQ−2.9 to FMQ+0.4. The latter are generally lower in fO_2, consistent with the results that they on average have higher Fe-loss. The fO_2 difference would be ascribed to their differences in the pressure assemblages and/or the amounts of initial Fe^{3+} in samples.

3.4. Fe-loss

Fe-loss (relative to initial Fe) was estimated for all the runs based on mass-balance calculations (Table 2). Two runs with $Au_{95}Cu_{05}$ capsules (D-8 and D-11) and 14 runs with $Pt_{95}Cu_{05}$ capsules had no Fe-loss or only small Fe-loss (<∼20% relative), but the other 11 runs with $Pt_{95}Cu_{05}$ capsules experienced >20% Fe-loss (4 runs with 20–50% loss and 7 runs with >50% loss). Most of the runs used $Pt_{95}Cu_{05}$ rather than $Au_{95}Cu_{05}$ capsules because AuCu alloy has a relatively low melting point and oxygen buffer materials such as Ni easily form alloy with Au leading to much lower melting points. Our exploratory experiments showed that $Au_{95}Cu_{05}$ capsules melted when temperature was higher than 900 °C if Ni–NiO buffer was used.

Fe-loss with $Pt_{95}Cu_{05}$ capsules appears to be mainly fO_2 dependent, although temperature and duration also have effects. For the MORB and K-basalt runs, 8 runs show nearly no Fe-loss (⩽3%) and 3 runs show severe Fe-loss (59–78%). For the dacite runs, nearly all the runs had a different extent of Fe-loss (>10%) and 3 runs had Fe-loss >90%. The higher Fe-losses for the dacite runs coincide with their lower fO_2 (<FMQ+0.4) and lower melt Cu solubility (<800 ppm). These results demonstrate that Fe-loss with $Pt_{95}Cu_{05}$ capsules was quite severe at reducing

conditions. Fe-loss has resulted in high Mg# values in minerals and melts for some runs. And it also affects the mineral/melt Fe–Mg exchange distribution coefficients (K_D) calculated if the minerals were not re-equilibrated to the melts. Detailed discussions on how Fe-loss affect Mg# and K_D and whether or not Fe-loss affect the Cu partitioning are given in Sections 3.5 and 4.1.

3.5. Mineral compositions and mineral/melt Cu partitioning

3.5.1. Olivine

Olivines crystallized only in three K-basalt runs: K-3, K-6 and K-7 (Table 2). They are euhedral and the compositions in single run are very homogeneous (Table S3), indicating equilibrium crystallization. These olivines have Mg# values of 90–97. The high Mg# values are not a result of Fe-loss since only run K-3 has Fe-loss (16%) and because Fe-loss should result in higher Mg# calculated but the Mg# of 90 in olivine from this run is lowest among the three runs. The high Mg# values could be attributed to the relatively high fO_2 in the three runs (>FMQ+1.2, Table 2). The high fO_2 resulted in low Fe^{2+}/Fe^{3+} and thus high Mg^{2+}/Fe^{2+} in the melts. Olivines crystallized from such high Mg^{2+}/Fe^{2+} melts must have high Mg# values. This explanation is consistent with that olivine Mg# value increases with increasing fO_2 (K-3: 90 Mg# vs. FMQ+1.2; K-7: 94 Mg# vs. FMQ+2.7; K-6: 97 Mg# vs. FMQ+4.4) at the same T (1000 °C) and melt composition ($X_{nf}/X = \sim 0.60$).

With the EMP analyses of FeOt and MgO, the calculated olivine/melt Fe–Mg exchange distribution coefficients $[K_D^{ol} = (X_{Fe}^{ol}/X_{Mg}^{ol}) \cdot (X_{Mg}^{lid}/X_{Fe}^{lid})]$ in runs K-3, K-6 and K-7 are 0.19, 0.07 and 0.13, respectively. The three runs had olivine–spinel equilibrium fO_2 values at FMQ+1.2, FMQ+4.4 and FMQ+2.7, respectively (Table 2). Using these fO_2 values and the model of Kress and Carmichael (1991), we calculated Fe^{2+} contents in the melts and then the K_D values for the three runs were respectively corrected to 0.22, 0.19 and 0.21. These values are close to a constant value of 0.21 ± 0.02, indicating olivine/melt Fe–Mg exchange equilibrium. Note that this constant value is a bit lower than the olivine/melt Fe–Mg K_D values of 0.26–0.30 (Hirose and Kawamoto, 1995), 0.34 (Gaetani and Grove, 1998) and 0.35 (Walter, 1998) from peridotite and basalt experiments. The reason for the difference could be attributed to the andesitic melt compositions of our experiments (with melt becoming more felsic, $X_{Mg}^{lid}/X_{Fe}^{lid}$ will decrease and thus K_D must decrease). Also note that although run K-3 had 16% Fe-loss, its fO_2-Fe^{2+}-corrected K_D value is nearly identical to those of runs K-6 and K-7 where no Fe-loss occurred. This implies that either <20% Fe loss would not affect the K_D value much or the olivines in K-3 re-equilibrated to the melt during Fe-loss occurred.

Cu contents in olivines are 166–1438 ppm in the three runs and the olivine/melt Cu partition coefficients ($D_{Cu}^{ol/melt}$) range from 0.113 ± 0.018 to 0.202 ± 0.003 (Table S3) and increase with increasing fO_2 (Fig. 4a). This trend is consistent with the observation of Liu et al. (2014). It implies that Cu^{2+}/Cu^{1+} ratio in the melts increased with increasing fO_2 (although Cu^{1+} was still dominant) because Cu^{2+} (0.73 Å) should more easily substitute Mg^{2+} (0.72 Å) and Fe^{2+} (0.78 Å) in the octahedral sites of olivine structure. The inferred presence of Cu^{2+} at our relatively high fO_2 conditions is consistent with a formal Cu valence state in melt of 1.28 predicted based on the correlation between Cu solubility and fO_2 (see Section 3.2.2). It can also be seen from Fig. 4a that at a given fO_2 value, $D_{Cu}^{ol/melt}$ for the K-basalt runs (1000 °C) is higher than that for the Komatiite runs (1250–1300 °C) of Liu et al. (2014), suggesting that temperature has a substantial effect on the Cu partitioning, although a slight effect of melt composition cannot be excluded.

Compared to the previous data, the $D_{Cu}^{ol/melt}$ values of this study (0.11–0.20) and Liu et al. (2014) (0.04–0.14) are generally comparable to those (0.02–0.071) obtained by Audétat and Pettke (2006) and those (0.03–0.15) obtained by Lee et al. (2012) with in-situ LA-ICP-MS analysis of natural samples, and those (0.08–0.19) obtained by Gaetani and Grove (1997) and those (0.06–0.21) obtained by Fellows and Canil (2012) in laboratory experiments. However, they are one order of magnitude lower than those (1.2–4.1) experimentally obtained by Adam and Green (2006). As pointed out by Adam and Green (2006), Liu et al. (2014) conducted experiments with Cu-free noble metal capsules, which may have led to Cu partitioning disequilibrium in their experiments.

3.5.2. Opx

Opxs were encountered in two dacite runs (D-2 and D-8). They contain some Al_2O_3, CaO and minor TiO_2 and Cr_2O_3 in addition to SiO_2, MgO and FeO, and have Mg# values of 62 and 72. The opx/melt Fe–Mg K_D values are 0.61 and 0.12 (Table S3), respectively. Run D-2 had 54% Fe-loss (Table 2) and $K_D = 0.61$ for this run would be a bit higher than expected, probably indicating that the Fe–Mg exchange somewhat deviated equilibrium due to the relatively low initial H_2O (6%) and relatively short run duration (80 h). Run D-8 had no Fe-loss and we consider that its opx/melt K_D value of 0.12 (or the fO_2–Fe^{2+}-corrected value of 0.13) is likely a value approaching equilibrium for the very felsic melt composition ($X_{nf}/X = 0.80$) of this run, although this value appears to be lower than the literature value of ~0.30 in mafic systems (e.g., Gaetani and Grove, 1998).

Cu content in opx is 55 ppm in run D-2 and 14 ppm in run D-8 and the corresponding opx/melt D_{Cu} value is 0.246 ± 0.006 and 0.121 ± 0.024. These two opx/melt D_{Cu} values show to be higher than those (0.04–0.06) of Yao et al. (2012), those (0.06) of Sun and Liang (2013) and those (0.04–0.08) of Liu et al. (2014) experimentally obtained from mafic systems at much higher temperatures, suggesting that $D_{Cu}^{opx/melt}$, just like $D_{Cu}^{ol/melt}$, increases with decreasing temperature.

3.5.3. Cpx

Cpxs were present in seven MORB runs, two K-basalt runs and eight dacite runs. Cpx compositions in individual runs (except D-4, Table S4) are quite homogeneous but vary with experimental starting composition and P–T conditions. The cpxs ($Wo_{49-52}En_{41-51}Fs_{0-10}$) that crystallized from the MORB composition are Ca-rich (~22.5 wt.%

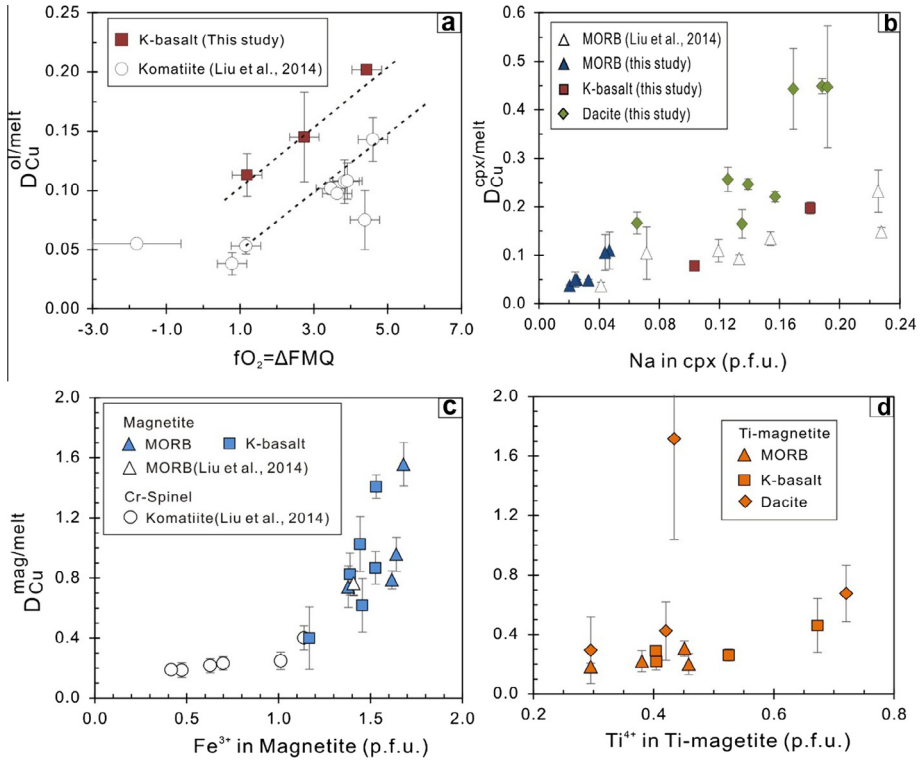

Fig. 4. Mineral/melt D_{Cu} values for olivine (a), cpx (b), magnetite (c) and Ti-magnetite (d). (a) D_{Cu} for olivine increases with fO_2 (when $fO_2 > \sim\Delta$FMQ+1) and at a given fO_2, D_{Cu} from the K-basalt experiments (1000 °C, this study) is higher than that from the Komatiite experiments (1250–1300 °C, Liu et al., 2014). (b) D_{Cu} for cpx from the dacite experiments (950–1000 °C, this study) are generally higher than those from the MORB experiments (1150–1250 °C, Liu et al., 2014) at a given Na (pfu) in cpx. (c) D_{Cu} for magnetite, with data for Cr-spinel from the Komatiite experiments (Liu et al., 2014) shown for comparison. (d) D_{Cu} for T-magnetite. Fig. (c) and (d) show that (1) D_{Cu} for magnetite increases with Fe^{3+} (pfu) in magnetite, whereas D_{Cu} for titanomagnetite slightly increases with Ti^{4+} (pfu) in titanomagnetite, and (2) magnetite/melt D_{Cu} values are generally higher than those of titanomagnetite/melt (if the unusual Ti-magnetite value excluded).

CaO) but Na-poor (0.29–0.71 wt.%) and contain 0.38–0.93 wt.% TiO_2, whereas those ($Wo_{44-48}En_{39-53}Fs_{0-16}$) that crystallized from the dacite composition are relatively Ca-poor (15.60–18.12 wt.% CaO) but Na-rich (0.94–2.75 wt.%) and contain 0.30–1.09 wt.% TiO_2. Compositions ($Wo_{45-50}En_{38-44}Fs_{11}$) of the cpxs from two K-basalt runs are between those from the MORB and dacite runs. Excluding the four severe Fe-loss runs (M-1, M-4, D-4 and D-6), the Mg# values of cpxs from the MORB and K-basalt runs are 65 to 82 and from the dacite runs are 62 to 77. The cpx/melt Fe–Mg K_D value, calculated with Fe in cpx as Fe^{2+}, is 0.48 ± 0.13 (0.31–0.55) for the MORB and K-basalt runs and 0.44 ± 0.19 (0.11–0.66) for the dacite runs. These values are generally higher than the literature values of 0.35 ± 0.05 (Hirose and Kawamoto, 1995) and 0.36 ± 0.04 (Kinzler, 1997), but overlap those of 0.45 ± 0.07 and 0.49 ± 0.05 (Pichavant et al., 2002). The fluctuant K_D values in our experiments are more or less ascribed to the different degree of Fe-loss.

For the four runs with severe Fe-losses, M-1 and M-4 have cpx/melt Fe–Mg K_D values respectively at 0.40 and 0.31 close to the average value of 0.48 ± 0.13 for cpxs in the MORB samples and D-6 has cpx/melt Fe–Mg K_D value at 0.57 in the range of 0.44 ± 0.19 for cpxs in the dacite samples. Cpx/melt Fe–Mg exchange in these runs are thus considered to be close to equilibrium. Their unusually high Mg# values (90–99) are attributed to significant amounts of Fe-loss that occurred earlier than cpx crystallization. Fe-loss led to high MgO/FeO ratios in melts and thus cpxs crystallized from these Fe-depleted melts must have high Mg#. Only the cpx from run D-4 had a relatively large S.D. value of FeO analyses and an unusually high K_D value of 3.14 (Table S4), indicating disequilibrium crystallization.

Cu content of cpxs range from 13 to 437 ppm. The cpx/melt D_{Cu} values are given in Table S4 and shown in Fig. 4b. Seven MORB runs give the values of 0.038 ± 0.002 to 0.182 ± 0.053, two K-basalt runs give the values of 0.078 ± 0.006 and 0.197 ± 0.012, and eight dacite runs give the values of 0.165 ± 0.030 to 0.449 ± 0.016. Cpx composition has a pronounced effect on the Cu partitioning. As shown in Fig. 4b, the D_{Cu} value for a same (MORB, K-basalt or dacite) series of runs obviously increases with increasing Na (pfu) in cpx. This trend implies that the behavior of Cu in cpx is similar to Na (Liu et al., 2014) and that Cu^+ substitution in addition to the Cu^{2+} substitution may be present in the cpx structure, explaining D_{Cu} values (up to 0.45) for cpx/melt higher than those ($<\sim$0.2)

for olivine/melt and opx/melt. At a given Na in cpx (pfu), D_{Cu} values of dacite samples obtained in this study (950–1100 °C) appear to be generally higher than those of MORB samples from Liu et al. (2014) obtained at higher temperatures (1150–1250 °C), again indicating a significant effect of temperature on the Cu partitioning.

For Cu partitioning between cpx and basaltic–andesitic to dacitic melts, no experimental data from literature are available. Our D_{Cu} values (0.038–0.197) for the MORB and K-basalt runs overlap those (0.05–0.08) of Dostal et al. (1983) and those (0.01–0.07) of Audétat and Pettke (2006) from natural basaltic–andesitic samples. The D_{Cu} values (0.165–0.449) for the dacite experiments are lower than those (0.51–0.87) of Ewart et al. (1973) for natural dacite samples and those (0.80–2.20) of Ewart and Griffin (1994) for natural low silica rhyolite samples.

3.5.4. Amphibole

Amphiboles were present in one MORB run (M-5), six K-basalt runs and three dacite runs. Composition of amphiboles in individual runs (except for run D-10, Table S5) is homogeneous, indicating equilibrium crystallization. All the amphiboles are pargasites with compositions varying slightly with the variation of starting composition. The amphiboles that crystallized from the K-basalt composition are slightly lower in SiO_2 (42–44 wt.%) and higher in K_2O (0.7–1.1 wt.%) relative to those from the dacite runs (42–47 wt.% SiO_2 and ~0.35 wt.% K_2O). The amphibole that crystallized from the MORB composition has the lowest K_2O content (0.14 wt.%). All amphiboles have Mg# values between 55 and 79. The amphibole/melt Fe–Mg exchange K_D is 0.47 ± 0.05 for the K-basalt runs and 0.27 ± 0.08 for the dacite runs. The difference in the K_D values should be ascribed to the difference in their melt compositions. An exception is run D-10, where amphibole has Mg# of 93 and K_D of 1.18 due to severe Fe-losses (93%), and indicating disequilibrium crystallization of amphibole in this run.

Amphiboles have Cu content in the range of 1.8 to 210 ppm and amphibole/melt D_{Cu} values are reported in Table S5. The MORB run (M-5) gives a value of 0.127 ± 0.006. Six K-basalt runs give values of 0.035 ± 0.002 to 0.197 ± 0.068, and three dacite runs give values of 0.082 ± 0.012 to 0.124 ± 0.013. All the 10 amphibole/melt D_{Cu} values are lower than 0.20 (0.035 to 0.197). No literature data on experimental amphibole/melt D_{Cu} values in intermediate to felsic systems are available. Our amphibole/melt D_{Cu} values (0.04 to 0.20) overlap with those (0.05) of Dostal et al. (1983) obtained from a natural basaltic andesite, but are lower than those (0.50–1.50) of Ewart and Griffin (1994) obtained from natural dacites and rhyolites. We are suspicious of the Cu partitioning results on natural samples (ol/melt up to 2.7, cpx/melt up to 2.2 and amph/melt up to 1.5) of Ewart and Griffin (1994), who used the proton microprobe to determine the Cu content in minerals and melts. Their results are not consistent with the results of Halter et al. (2004), Audétat and Pettke (2006) and Lee et al. (2012) with in-situ LA-ICP-MS analysis of natural samples (see Table S1) and with our experimental results in this study.

3.5.5. Garnet

Garnets (usually >50 μm and up to 200 μm) were present in two K-basalt runs (2.0 GPa) and five dacite runs (2.0–2.5 GPa). Their compositions are reported in Table S6. Garnets are dominantly of mixed pyrope, almandine and grossular compositions and contain minor TiO_2, MnO and Na_2O. Garnets from the K-basalt runs are slightly MgO-rich (Mg# = 71–75) relative to those from the dacite runs (Mg# = 49–69). All the garnets have compositional zoning with cores relative to rims slightly rich in MgO and poor in FeO, although they are homogeneous in SiO_2, Al_2O_3 and CaO. Garnet-rim/melt Fe–Mg K_D values vary between 0.50 and 1.50 with an exception of 8.30 for run D-4. The relatively big variation range of garnet-rim/melt K_D values indicate that the growing of garnet was very fast and Fe-loss kept going after garnet crystallization, resulting in disequilibrium of the Fe–Mg exchange for this phase.

Garnet has the lowest Cu content (1.4–28.7 ppm) among all the investigated minerals. D_{Cu} values between garnet rims and coexisting melts were determined. All these values are lower than 0.08. D_{Cu} values (Table S6) from the K-basalt runs are 0.007 ± 0.002 to 0.027 ± 0.006, and these from the dacite runs are 0.024 ± 0.014 to 0.064 ± 0.008. These results are comparable to the garnet/melt D_{Cu} values of 0.04–0.05 from the MORB experiments of Liu et al. (2014). They are also comparable to the garnet/melt D_{Cu} values of 0.004 (Lee et al., 2012) and 0.08 (Fulmer et al., 2010) obtained from natural samples. All these D_{Cu} values confirm that garnet behaves most incompatibly with respect to Cu among all mafic minerals.

3.5.6. Plagioclase

Only D-8 (1.0 GPa, 950 °C) from the dacite experiments produced plagioclase ($An_{36}Ab_{62}Or_2$). The plagioclase/melt D_{Cu} value is 0.115 ± 0.027 (Table S6), moderately higher than the value of 0.023 ± 0.009 for plagioclase ($An_{62}Ab_{38}Or_{0.4}$) from the MORB run (1.0 GPa, 1150 °C) of Liu et al. (2014).

3.5.7. Fe–Ti oxides

Fe–Ti oxides produced in this study include spinel group minerals, ilmenite and rutile. All these minerals are generally smaller than 10 μm, and thus their compositions including CuO (Table S7) were determined only by EMPA. Ilmenite and rutile were found only in runs D-8 and D-14Ti, respectively. The estimated D_{Cu} values are 0.32 for ilmenite/melt and 0.05 for rutile/melt. However, these values should be regarded as maximum values, since CuO contents in these two minerals are below 0.01 wt.% and the EMP analyses may give artificially higher CuO contents when CuO below 0.02 wt.% according to Fig. 1. Based on their Fe, Ti, and Cr contents, the spinel group minerals from this study can be divided into three distinct populations: magnetite, titanomagnetite and Cr-spinel. Their compositions and mineral/melt Cu partitioning are summarized as follows:

Magnetites crystallized in four MORB runs and six K-basalt runs (Table 2). Magnetite compositions (Table S7) from these two series of experiments overlap.

They are mainly composed of FeO (FeOt: 61.73–78.31 wt.%), Al_2O_3 (6.28–11.25 wt.%) and MgO (7.34–15.26 wt.%), mostly containing < 2.0 wt.% of TiO_2 and Cr_2O_3. Therefore, they have compositions mainly along the $FeFe_2O_4$–$MgAl_2O_4$ (magnetite–spinel) solid-solution join. These magnetites coexisted with intermediate melts. Magnetites have CuO contents in the range of 0.025–1.18 wt.%. Their mineral/melt D_{Cu} values range from 0.400 ± 0.208 to 1.558 ± 0.113 (Table S7) and increases with increasing Fe^{3+} (pfu) in magnetite (Fig. 4c). This trend is in agreement with that spinel/melt D_{Cu} value increases with increasing fO_2 and Fe^{3+} (pfu) in Cr- and Al-rich spinel (Liu et al., 2014). Such increase is possibly related to $Cu^+ + Fe^{3+} = 2\ Fe^{2+}$ (or Mg^{2+}) substitution in magnetite. Our magnetite/melt D_{Cu} values (0.4–1.6) are comparable to those (0.82–2.0) obtained experimentally by Simon et al. (2006, 2008) and those (0.17–0.63) obtained from natural samples by Audétat and Pettke (2006).

Titanomagnetites crystallized in four MORB runs, four K-basalt runs and five dacite runs (Table 2). Titanomagnetite compositions (Table S7) from these three series of experiments cannot be clearly distinguished. They are TiO_2- and FeOt -rich (TiO_2: 9.92–25.24 wt.%, FeOt: 62.42–76.42 wt.%) and contain minor contents of MgO (1.0–5.0 wt.%), Al_2O_3 (1.65–3.55 wt.%) and Cr_2O_3 (<2.0 wt.%). Titanomagnetite usually coexisted with magnetite in an individual run in the MORB and K-basalt experiments. In this case, titanomagnetite can be clearly distinguished from magnetite in terms of its much higher TiO_2 and relatively lower MgO and Al_2O_3. Such Fe- and Ti-based characteristics indicate that they are the solid-solutions along $FeFe_2O_4$–Fe_2TiO_4 (magnetite–ulvöspinel) join. Titanomagnetites have CuO content ranging from 0.019 to 0.24 wt.%. The titanomagnetite/melt D_{Cu} values are in the range of 0.185 ± 0.020 to 0.676 ± 0.188 (Table S7), generally lower than those (0.40–1.6) for magnetites (Fig. 4c vs. d). An exception is the titanomagnetite from run D-8, which has an unusually high D_{Cu} value at 1.715 ± 0.667. In general, titanomagnetite/melt D_{Cu} value appears to increase slightly with TiO_2 (or Ti^{4+}/pfu) in this phase (Fig. 4d), indicating possible presence of a substitution $Cu^+ + Ti^{4+} = Fe^{3+} + Fe^{2+}$ (or Mg^{2+}). Our titanomagnetite/melt D_{Cu} values (~0.20 to 1.72) are significantly lower than those (26 ± 17) obtained experimentally by Simon et al. (2008) in rhyolitic melt. The difference might be caused by the different melt compositions and/or temperatures used in these two studies.

Cr-spinels (Table S7) were encountered only in one K-basalt run (K-8Ti) and two dacite runs (D-2 and D-7). They contain high contents of Cr_2O_3 (22.85–48.89 wt.%) and FeO (24.34–51.44 wt.%), and also some Al_2O_3 (14.72–14.93 wt.%) and MgO (5.00–7.40 wt.%) but minor TiO_2 (<2.0 wt.%). They thus are the solid-solutions of $FeCr_2O_4$–$FeFe_2O_4$–$MgAl_2O_4$ (chromite–magnetite–spinel) triangle. These Cr-spinels contain 0.027–0.94 wt.% CuO. The Cr-spinel/melt D_{Cu} values in these runs are 0.973 ± 0.218 to 1.831 ± 0.735 (Table S7), higher than those (<0.40) for Cr-rich spinels from the Komatiite experiments (Liu et al., 2014). The difference is mainly attributed to the much lower temperatures in the K-basalt and dacite runs (2.0 GPa, 1000 °C) than in the Komatiite runs (1.0 GPa, 1250–1300 °C).

3.5.8. Summary of the Cu partitioning

A total of 99 mineral/melt Cu partition coefficients (including 26 values from Liu et al., 2014) for silicate minerals and oxide minerals were obtained experimentally with Cu-bearing Pt or Au capsules with komatiitic–basaltic–dacitic compositions under the P–T–fO_2 conditions of upper mantle to crust. These D_{Cu} values include 12 olivine/, 5 opx/, 26 cpx/, 10 amphibole/, 9 garnet/, 2 plagioclase/, and 35 oxides/(12 magnetite, 13 titanomagnetite and 10 Cr-spinel)/melt pairs.

All the mineral/melt D_{Cu} values are summarized in Table 3 and Fig. 5. As shown in Fig. 5, our D_{Cu} values for individual minerals are generally comparable to the natural phenocryst/melt D_{Cu} values that were determined with LA-ICP-MS methods, but lower than or only overlap the lower ends of previous experimental D_{Cu} values.

The general order of mineral/melt D_{Cu} values is garnet (0.007–0.064) ⩽ plagioclase (0.02–0.12) ⩽ olivine (0.04–0.20) ≈ opx (0.04–0.24) ≈ amphibole (0.04–0.20) ⩽ cpx (0.04–0.45) ⩽ magnetite, titanomagnetite and Cr-spinel (0.18–1.83). These D_{Cu} values indicate that Cu is generally highly incompatible in mafic minerals, and is incompatible to moderately compatible in Fe–Ti oxides (magnetite, titanomagnetite and Cr-spinel). The variations of the D_{Cu} values depend mainly on temperature, fO_2 and/or mineral composition. In general, D_{Cu} for olivine (and perhaps opx) increases with decreasing temperature and increasing fO_2. Cpx/melt D_{Cu} value increases with increasing Na^+ (pfu) in cpx; magnetite/melt and Cr-spinel/melt D_{Cu} values increase with increasing Fe^{3+} (pfu) in these two minerals; titanomagnetite/melt D_{Cu} value increases with increasing Ti^{4+} (pfu) in titanomagnetite.

4. DISCUSSION

4.1. Chemical equilibrium

4.1.1. Major elements

In Section 3.5, chemical equilibrium of major elements for the specific minerals in individual runs were discussed based on mineral morphology, phase composition and mineral/melt Fe–Mg K_D value. We here only summarize the results: (1) The euhedral habitus of most mafic minerals and subhedral habitus of Fe–Ti oxides (Fig. 2) indicate their crystallization close to equilibrium. (2) Most of the minerals and all the melts are compositionally homogeneous, as indicated by EMP analyses (Tables S2–S7). Limited compositional zoning was found only in the garnets, and compositional inhomogeneity was only observed in opx from run D-2, cpx from run D-4 and amphibole from run D-10. (3) 16 runs have no or only small (<~20%) Fe-loss. Mafic minerals except garnets in these runs have nearly constant Fe–Mg K_D values, indicating Fe–Mg exchange approaching equilibrium in the 16 runs. 11 relatively reducing runs (Table 2: two MORB runs, one K-basalt runs and eight dacite runs) have Fe-loss >20%, resulting in more or less elevation in Mg# value of the mafic

Table 3
Mineral/melt Cu partition coefficients.

Sample.	ol	s.d.	opx	s.d.	cpx	s.d.	grt	s.d.	amp	s.d.	Cr-spl	s.d.	mag	s.d.	Ti-mag	s.d.	pl	s.d.
Starting material: Komatiite (1.0 GPa, 1250–1300 °C, komatiitic–basaltic melts)																		
Cu-50*	0.055	0.003	0.036	0.005														
Cu-46*	0.107	0.018									0.232	0.044						
Cu-31*	0.097	0.004									0.186	0.048						
Cu-5*	0.074	0.025									0.248	0.057						
Cu-30*	0.108	0.015									0.217	0.047						
Cu-55*	0.102	0.005									0.189	0.024						
Komatiite-L4*	0.053	0.007	0.039	0.007	0.060	0.008					0.203†	0.107						
Komatiite-L2*	0.038	0.009									0.246†	0.104						
Komatiite-L1*	0.143	0.019	0.094	0.012	0.066	0.012							0.401	0.081				
Starting material: MORB (0.5–3.5 GPa, 950–1250 °C, basaltic–andesitic melts)																		
MORB-L2*					0.110	0.023												
MORB-L1*					0.093	0.009												
MORB-L3*					0.134	0.014												
MORB-L5*					0.232	0.044	0.046	0.007										
MORB-L6*					0.148	0.009	0.038	0.004										
Cu-41*					0.038	0.006											0.023	0.009
Cu-6*					0.105	0.054							0.765	0.06				
M-1					0.049	0.002												
M-2					0.182	0.058							0.788	0.138				
M-3					0.110	0.038							0.741	0.143	0.201	0.070		
M-4					0.038	0.002												
M-5					0.106	0.037			0.127	0.006					0.221	0.070		
M-6					0.050	0.001							1.558	0.113	0.185	0.020		
M-7					0.050	0.015							0.958	0.107	0.306	0.051		
Starting material: K-basalt (0.5–2.0 GPa, 950–1000 °C, andesitic melts)																		
K-1					0.078	0.006	0.007	0.002	0.035	0.001								
K-2									0.081	0.007			0.826	0.140	0.262	0.041		
K-3	0.113	0.018							0.048	0.003			0.618	0.178				
K-4									0.043	0.006			0.400	0.208				
K-5									0.173	0.070			1.027	0.183	0.219	0.057		
K-6	0.202	0.003											1.409	0.078	0.291	0.030		
K-7	0.145	0.038											0.868	0.109				
K-8Ti					0.197	0.012	0.027	0.006	0.141	0.018	1.318	0.372			0.460	0.182		
Starting material: Dacite (1.0–2.5 GPa, 950–1000 °C, dacitic–rhyolitic melts)																		
D-1							0.030	0.007										
D-2			0.246	0.006	0.449	0.016					0.973	0.325						
D-3					0.443	0.083	0.036	0.007							0.425	0.196		
D-4					0.256	0.025	0.064	0.008										
D-5					0.221	0.011	0.027	0.020										
D-6					0.165	0.030												

Table 3 (*continued*)

Sample.	ol	s.d.	opx	s.d.	cpx	s.d.	grt	s.d.	amp	s.d.	Cr-spl	s.d.	mag	s.d.	Ti-mag	s.d.	pl	s.d.
D-7					0.447	0.126	0.048	0.014			1.831	0.735						
D-8			0.121	0.024	0.166	0.022									1.715	0.677	0.115	0.027
D-9									0.124	0.013					0.294	0.223		
D-10									0.082	0.012								
D-11									0.104	0.027								
D-12															0.499	0.511		
D-14Ti					0.246	0.011									0.676	0.188		

* From Liu et al., 2014, others from Tables S3–S7 in this study; mineral abbreviations as in Table 2.

† Cr-spinel/melt D_{Cu} values in these two experiments were determined in this study; s.d.: standard deviation.

minerals and melts. However, most of minerals from these runs (except garnet in four runs, opx in D-2, cpx in D-4 and amphibole in D-10) are still compositionally homogeneous and their Fe–Mg K_D values have only very slight deviations to the average values, thus indicating that Fe–Mg exchange in most of the runs with considerable Fe-loss also roughly approached equilibrium. These results demonstrate that for most of the Fe-loss runs, the mineral crystals have re-equilibrated quite closely to the melts as they were losing Fe, and Fe-loss for these runs did not significantly affect mineral–melt Fe–Mg exchange equilibrium.

4.1.2. Cu partitioning

Assessment of Cu partitioning equilibrium can be made from observations of the homogeneity of Cu concentration in run products (minerals and melts) and by considering whether Cu partitioning varies systematically with experimental conditions. Cu analyses of all the minerals and melts (Tables S2–S7) have low standard deviations (S.D.), indicating that Cu concentration in each phase of any single run is homogeneous, and that the diffusion of Cu^{1+} (low charge and ionic radius) in melt was very fast and the diffusion equilibrium was achieved. The calculated mineral/melt D_{Cu} values for most of the minerals vary systematically with temperature, mineral composition or fO_2 (Section 3.5). These suggest that Cu partitioning in our experiments approached equilibrium.

Note that mafic minerals that crystallized from the runs that experienced Fe-loss usually have higher Mg# values than expected. However, as Mg^{2+} and Fe^{2+} mix almost ideally in most minerals and melts, trace element partition coefficients are expected to remain relatively constant with changing Mg# (e.g., O'Neill et al., 2003; Toplis, 2005). Liu et al. (2014) confirmed that at least olivine/, opx/ and cpx/melt Cu D_{Cu} values are not related to their Mg-numbers. Also note that it is difficult to demonstrate the accuracy of D_{Cu} values for garnet/melt pairs and for opx/melt in run D-2, cpx/melt in run D-4 and amphibole/melt in run D-10 due to their major element dis-equilibration (see above). However, the D_{Cu} values for the phases are comparable to those from natural samples (see Section 3.5.5 for garnet) or are in the D_{Cu} ranges of other runs for a same series of experiments, which indicates that these D_{Cu} values yield at least reasonable approximations even if their Fe–Mg exchanges were in disequilibrium. Our work demonstrates that using Pt–Cu alloy capsules have obtained more accurate Cu partition coefficients, although such capsules would result in Fe–Mg exchange disequilibrium at reducing conditions due to Fe-loss.

Finally, it should be pointed out that Henry's law may not be a problem in this study. Although the concentrations of Cu in the minerals and melts in some runs are up to several thousand ppm which are much higher than those in natural systems, the D_{Cu} values for olivine, opx, cpx, garnet, amphibole, spinel and magnetite from this study agree with or are comparable to those obtained with in-situ LA-ICP-MS analysis of natural samples (e.g., Halter et al., 2004; Audétat and Pettke, 2006; Lee et al., 2012). This suggests that the Cu partitioning of this study follows Henry's law.

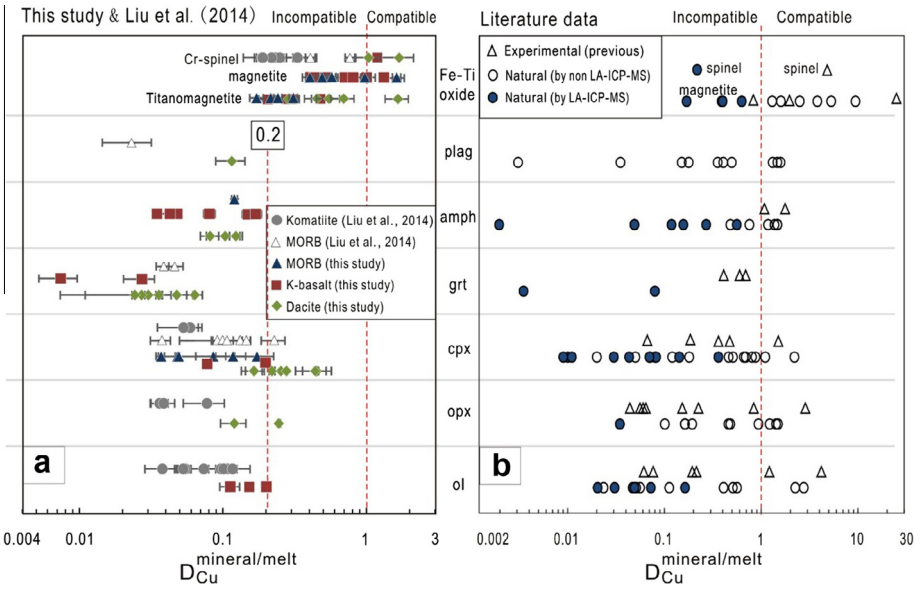

Fig. 5. A contrast of mineral/melt D_{Cu} values from this study and Liu et al. (2014) (a) to the literature data (b) (see text for the details). Mineral abbreviations as in Table 2. Literature data (see Tables S1 for the details): Experimental (previous): Adam and Green (2006), Dygert et al., 2014, Fellows and Canil (2012), Gaetani and Grove (1997), Hart and Dunn (1993), Klemme et al. (2006), Simon et al. (2006, 2008), Yurimoto and Ohtani (1992). Sun and Liang (2013) and Yao et al. (2012); Natural (by non-LA-ICP-MS): Natural phenocryst-matrix D_{Cu} values (measured by non-LA-ICP-MS) from Bougault and Hekinian (1974), De Hoog et al. (2001), Dostal et al. (1983), Ewart et al. (1973), Ewart and Griffin (1994), Kloeck and Palme (1987), Liotard et al. (1982), Paster et al. (1974) and Pedersen (1979); Natural (by LA-ICP-MS): Natural phenocryst-matrix (melt inclusion) D_{Cu} values (measured by LA-ICP-MS) from Audétat and Pettke (2006), Fulmer et al. (2010), Halter et al. (2004), Lee et al. (2012), Ubide et al. (2014), Zack and Brumm (1998) and Zajacz and Halter (2007).

4.2. Effects of S and Cl on Cu partitioning?

In this study, dissolution of Cu in silicate melt is considered as Cu–O complex. However, if the dissolution not only as Cu–O complex but also as Cu–S and/or Cu–Cl complexes, then the effects of S and Cl on Cu partitioning have to be considered. The complex types and valence states of Cu dissolved in silicate melts have not been directly determined so far, but the solubility data obtained by Ripley and Brophy, 1995; Zajacz et al. (2012, 2013) and in this study indicate that Cu dissolved in silicate melts dominantly as Cu^{+} and perhaps in very minor amounts as Cu^{2+}. Zajacz et al. (2012, 2013) investigated the influences of S and Cl on Cu solubility in andesitic-rhyolitic melts. They found that Cu solubility is only slightly positively related to Cl or S content in the melts. This suggests that Cu dissolves in silicate melts dominantly as Cu–O complex while Cu–S and Cu–Cl complexes are not significant. Hence, S and Cl should not significantly affect Cu partitioning, especially in the levels of S and Cl concentrations of natural magmas. In this study, there are two points confirming that S and Cl have no substantial effects on the Cu partition coefficients: (1) Runs K-1 to K-8 are the experiments with a natural K-basalt, which would contain some S and Cl, but there is no evidence that shows Cu partitioning results of these runs are different from those in the runs with the S- and Cl-free synthetic compositions (MORB and dacite), and (2) the D_{Cu} values for olivine, opx, cpx, garnet, amphibole, spinel and magnetite from this study agree with or are comparable to those obtained with in-situ LA-ICP-MS analysis of natural samples (e.g., Halter et al., 2004; Audétat and Pettke, 2006; Lee et al., 2012).

5. APPLICATIONS

Metal-rich magmas are a favorable, albeit not sufficient, condition for the formation of magmatic-hydrothermal ore deposits. The magmas associated with porphyry Cu deposits are intermediate to felsic and are characterized by high Sr/Y ratios. Such magmas can be produced by fractional crystallization from H_2O-rich arc magmas (Richards, 2011; Chiaradia et al., 2012; Loucks, 2014) or partial melting of hydrous metabasalts at subducting slabs (Sun et al., 2011, 2013) or at the base of thickened continental crust (Hou et al., 2004; Wang et al., 2006; Richards, 2009; Shafiei et al., 2009). Whatever fractional crystallization or partial melting, the predecessor magmas/rocks to the intermediate-felsic magmas are mafic and the involved residual or fractional phases include amphibole ± garnet ± cpx + Fe–Ti oxides ± sulfides without plagioclase, sometimes possibly involving olivine and opx.

During magmatic processes, the behavior of Cu is controlled by the partitioning of Cu between the crystalline phases and derived melts. Our experiments here demonstrate that Cu is highly incompatible (D_{Cu} generally $<\sim 0.2$) in all the mafic minerals and is moderately incompatible to compatible ($D_{Cu} < 2.0$ and mostly <1.0) in Fe–Ti oxides. Because Fe–Ti oxides are minor phases in intermediate to felsic rocks, their contribution to the bulk solid/melt D_{Cu} is limited. Based on an amphibole-dominated

factional crystallization consisting of 30–60 wt.% amphibole, 10–20 wt.% cpx, 10–20 wt.% garnet and 2 wt.% magnetite and corresponding mineral/melt D_{Cu} values of 0.10, 0.40, 0.08 and 1.0, respectively, a bulk D_{Cu} of 0.16–0.18 is obtained for sulfide-absent factional crystallization. For partial melting of mafic rocks with a sulfide-free residue (granulite or eclogite) consisting of 20–50 wt.% garnet, 20–40 wt.% cpx, 5–10 wt.% amphibole and minor magnetite and rutile, a D_{Cu}^{bulk} of 0.20–0.22 is obtained. These estimated results indicate that the D_{Cu}^{bulk} values are around 0.2 for the sulfide-free assemblages. Therefore, Cu will be concentrated efficiently in the derived melts during fractional crystallization or partial melting in the absence of sulfides. Sulfide-free scenarios may be realistic for arc magmas since many of the magmas are oxidized and H_2O-rich, both which destabilize sulfides (Carroll and Rutherford, 1987; Jugo et al., 2005, 2010) or suppress sulfide crystallization (Richards, 2009, 2011). However, for the partial melting of metabasalts at subducting slabs or at the base of thickened continental crust, the production of Cu-rich magmas would require unusually high-fO_2 to destabilize sulfides, which is not proven. Future studies should pay particular attention to the effects of fO_2 and fS_2 on sulfide stability and Cu partitioning between sulfide and silicate melt during the deep partial melting to test whether or not this model is valid.

6. CONCLUSIONS

This study used $Pt_{95}Cu_{05}$ and $Au_{95}Cu_{05}$ alloy capsules as Cu sources to determine Cu partitioning between mafic minerals, Fe–Ti oxides, and intermediate to felsic melts at 0.5–2.5 GPa, 950–1100 °C and various fO_2 conditions. The results are $D_{Cu} = 0.01–0.06$ for garnet, 0.11–0.20 for olivine, 0.12–0.24 for opx, 0.04–0.20 for amphibole, 0.02–0.45 for cpx, and 0.18–1.83 for Fe–Ti oxides. These new data complement our previous dataset of Cu partitioning between olivine, opx, cpx, garnet, spinel and mafic melts at 1.0–3.5 GPa, 1150–1300 °C (Liu et al., 2014). Both two studies demonstrate that Cu is highly incompatible in mafic minerals, and is moderately incompatible to compatible in Fe–Ti oxides.

The new D_{Cu} data resolve previous discrepancies in experimental studies and serve as a foundation for quantitatively understanding the behavior of Cu during magmatic processes. Cu enrichment via magmatic processes is arguably a favorable condition for forming porphyry systems. The fractional crystallization or partial melting of mafic magmas (rocks) involves removal of or leaving assemblages of mafic minerals (amphibole, garnet and cpx) + Fe–Ti oxides ± sulfides. Calculations with the partitioning data obtained in this study indicates that sulfide-free assemblages have bulk D_{Cu} values around 0.2. Cu will thus be concentrated efficiently in the derived melts during these processes if sulfides are absent or negligible.

ACKNOWLEDGEMENTS

We would like to thank H. Schulze for the preparation of some polished sections, P.J. Lin and D. Krausse for help with the electron microprobe analyses, X.L. Tu for help with some LA-ICP-MS analyses. McCammon, H. Ni and L. Li for help during some experiments. The authors gratefully acknowledge the financial supports from the NBRP of China (2014CB440802), the NSF of China (41373061, 41121002 and 41173070), and the GIGCAS (Y234152001, SKLIG-JY-14-01) to X.L. Xiong and from the Bayerisches Geoinstitut to H. Keppler. Comments from Dr. V. Le Roux, two anonymous reviewers and the associate editor Dr. E.M. Ripley have helped to substantially improve the manuscript. This is contribution No. IS-1997 from GIGCAS.

APPENDIX A. SUPPLEMENTARY DATA

Supplementary data associated with this article can be found, in the online version, at http://dx.doi.org/10.1016/j.gca.2014.12.010.

REFERENCES

Adam J. and Green T. (2006) Trace element partitioning between mica-and amphibole-bearing garnet lherzolite and hydrous basanitic melt: 1. Experimental results and the investigation of controls on partitioning behaviour. *Contrib. Mineral. Petrol.* **152**, 1–17.

Audétat A. and Pettke T. (2006) Evolution of a porphyry-Cu mineralized magma system at Santa Rita, New Mexico (USA). *J. Petrol.* **47**, 2021–2046.

Audétat A. and Simon A. (2013) Magmatic controls on porphyry copper deposits. *Soc. Econ. Geol. Spec. Publ.* **16**, 553–572.

Ballhaus C., Berry R. F. and Green D. H. (1991) High pressure experimental calibration of the olivine–orthopyroxene–spinel oxygen geobarometer: implications for the oxidation state of the upper mantle. *Contrib. Mineral. Petrol.* **107**, 27–40.

Bell A. S., Simon A. and Guillong M. (2009) Experimental constraints on Pt, Pd and Au partitioning and fractionation in silicate melt–sulfide–oxide–aqueous fluid systems at 800°C, 150MPa and variable sulfur fugacity. *Geochim. Cosmochim. Acta* **73**, 5778–5792.

Bougault H. and Hekinian R. (1974) Rift valley in the Atlantic Ocean near 36°50′N: petrology and geochemistry of basaltic rocks. *Earth. Planet. Sci. Lett.* **24**, 249–261.

Carroll M. R. and Rutherford M. J. (1987) The stability of igneous anhydrite – experimental results and implications for sulfur behavior in the 1982 El-Chichon trachyandesite and other evolved magmas. *J. Petrol.* **28**, 781–801.

Chiaradia M., Ulianov A., Kouzmanov K. and Beate B. (2012) Why large porphyry Cu deposits like high Sr/Y magmas? *Sci. Rep.* **2**.

De Hoog J., Mason P. and Van Bergen M. (2001) Sulfur and chalcophile elements in subduction zones: constraints from a laser ablation ICP-MS study of melt inclusions from Galunggung Volcano. *Indonesia. Geochim. Cosmochim. Acta* **65**, 3147–3164.

Dostal J., Dupuy C., Carron J., Guen Le., de Kerneizon M. and Maury R. (1983) Partition coefficients of trace elements: application to volcanic rocks of St. Vincent. *West Indies. Geochim. Cosmochim. Acta* **47**, 525–533.

Dygert N., Liang Y., Sun C. and Hess P. (2014) An experimental study of trace element partitioning between augite and Fe-rich basalts. *Geochim. Cosmochim. Acta* **132**, 170–186.

Ewart A. and Griffin W. L. (1994) Application of proton-microprobe data to trace-element partitioning in volcanic rocks. *Chem. Geol.* **117**, 251–284.

Ewart A., Bryan W. and Gill J. (1973) Mineralogy and geochemistry of the younger volcanic islands of Tonga, SW Pacific. *J. Petrol.* **14**, 429–465.

Fellows S. A. and Canil D. (2012) Experimental study of the partitioning of Cu during partial melting of Earth's mantle. *Earth. Planet. Sci. Lett.* **337**, 133–143.

Fulmer E. C., Nebel O. and van Westrenen W. (2010) High-precision high field strength element partitioning between garnet, amphibole and alkaline melt from Kakanui, New Zealand. *Geochim. Cosmochim. Acta* **74**, 2741–2759.

Gaetani G. A. and Grove T. L. (1997) Partitioning of moderately siderophile elements among olivine, silicate melt, and sulfide melt: constraints on core formation in the Earth and Mars. *Geochim. Cosmochim. Acta* **61**, 1829–1846.

Gaetani G. A. and Grove T. L. (1998) The influence of water on melting of mantle peridotite. *Contrib. Mineral. Petrol.* **131**, 323–346.

Halter W. E., Pettke T. and Heinrich C. A. (2004) Laser-ablation ICP-MS analysis of silicate and sulfide melt inclusions in an andesitic complex I: analytical approach and data evaluation. *Contrib. Mineral. Petrol.* **147**, 385–396.

Hart S. R. and Dunn T. (1993) Experimental cpx/melt partitioning of 24 trace elements. *Contrib. Mineral. Petrol.* **113**, 1–8.

Hirose K. and Kawamoto T. (1995) Hydrous partial melting of lherzolite at 1 Gpa – the effect of H_2O on the genesis of basaltic magmas. *Earth Planet. Sci. Lett.* **133**, 463–473.

Holtz F., Johannes W., Tamic N. and Behrens H. (2001) Maximum and minimum water contents of granitic melts generated in the crust: a reevaluation and implications. *Lithos* **56**, 1–14.

Holzheid A. and Lodders K. (2001) Solubility of copper in silicate melts as function of oxygen and sulfur fugacities, temperature, and silicate composition. *Geochim. Cosmochim. Acta* **65**, 1933–1951.

Hou Z. Q., Gao Y. F., Qu X. M., Rui Z. Y. and Mo X. X. (2004) Origin of adakitic intrusives generated during mid-Miocene east–west extension in southern Tibet. *Earth. Planet. Sci. Lett.* **220**, 139–155.

Hou Z., Zhang H., Pan X. and Yang Z. (2011) Porphyry Cu (-Mo–Au) deposits related to melting of thickened mafic lower crust: examples from the eastern Tethyan metallogenic domain. *Ore Geol. Rev.* **39**, 21–45.

Jugo P. J., Candela P. A. and Piccoli P. M. (1999) Magmatic sulfides and Au:Cu ratios in porphyry deposits: an experimental study of copper and gold partitioning at 850 °C, 100 MPa in a haplogranitic melt–pyrrhotite–intermediate solid solution–gold metal assemblage, at gas saturation. *Lithos* **46**, 573–589.

Jugo P. J., Luth R. W. and Richards J. P. (2005) Experimental data on the speciation of sulfur as a function of oxygen fugacity in basaltic melts. *Geochim. Cosmochim. Acta* **69**, 497–503.

Jugo P. J., Wilke M. and Botcharnikov R. E. (2010) Sulfur K-edge XANES analysis of natural and synthetic basaltic glasses: implications for S speciation and S content as function of oxygen fugacity. *Geochim. Cosmochim. Acta* **74**, 5926–5938.

Kinzler R. J. (1997) Melting of mantle peridotite at pressures approaching the spinel to garnet transition: application to midocean ridge basalt petrogenesis. *J. Geophys. Res.* **102**, 853–874.

Kiseeva E. S. and Wood B. J. (2013) A simple model for chalcophile element partitioning between sulphide and silicate liquids with geochemical applications. *Earth. Planet. Sci. Lett.* **383**, 68–81.

Klemme S., Gunther D., Hametner K., Prowatke S. and Zack T. (2006) The partitioning of trace elements between ilmenite, ulvospinel, armalcolite and silicate melts with implications for the early differentiation of the moon. *Chem. Geol.* **234**, 251–263.

Kloeck W. and Palme H. (1987) Partitioning of siderophile and chalcophile elements between metal, sulfide, olivine, and glass in a naturally reduced basalt from Disko Island, Greenland. In *Lunar and Planetary Science Conference Proceedings*.

Kress V. C. and Carmichael I. S. E. (1991) The compressibility of silicate liquids containing Fe_2O_3 and the effect of composition, temperature, oxygen fugacity and pressure on their redox states. *Contrib. Mineral. Petrol.* **108**, 82–92.

Lee C. T. A., Luffi P., Chin E. J., Bouchet R., Dasgupta R., Morton D. M., Le Roux V., Yin Q. and Jin D. (2012) Copper systematics in arc magmas and implications for crust–mantle differentiation. *Science* **336**, 64–68.

Lepage L. D. (2003) ILMAT: an Excel worksheet for ilmenite–magnetite geothermometry and geobarometry. *Comput. Geosci.* **29**(5), 673–678.

Li Y. (2014) Comparative geochemistry of rhenium in oxidized arc magmas and MORB and rhenium partitioning during magmatic differentiation. *Chem. Geol.* **386**, 101–104.

Li Y. and Audétat A. (2012) Partitioning of V, Mn Co, Ni, Cu, Zn, As, Mo, Ag, Sn, Sb, W, Au, Pb, and Bi between sulfide phases and hydrous basanite melt at upper mantle conditions. *Earth. Planet. Sci. Lett.* **355–356**, 327–340.

Li Y. and Audétat A. (2013) Gold solubility and partitioning between sulfide liquid, monosulfide solid solution and hydrous mantle melts: Implications for the formation of Au-rich magmas and crust–mantle differentiation. *Geochim. Cosmochim. Acta* **118**, 247–262.

Liotard J., Dupuy C., Dostal J. and Cornen G. (1982) Geochemistry of the volcanic island of Annobon, Gulf of Guinea. *Chem. Geol.* **35**, 115–128.

Liu X., Xiong X., Audétat A., Li Y., Song M., Li L., Sun W. and Ding X. (2014) Partitioning of copper between olivine, orthopyroxene, clinopyroxene, spinel, garnet and silicate melts at upper mantle conditions. *Geochim. Cosmochim. Acta* **125**, 1–22.

Loucks R. (2014) Distinctive composition of copper-ore-forming arcmagmas. *Aust. J. Earth Sci.*, 1–13.

Nielsen R. (1990) Simulation of igneous differentiation processes. *Rev. Mineral. Geochem.* **24**, 65–105.

O'Neill H. S. C., Powneeby M. I. and McCammon C. A. (2003) The magnesiowüstite: iron equilibrium and its implications for the activity–composition relations of (Mg, Fe) $2SiO_4$ olivine solid solutions. *Contrib. Mineral. Petrol.* **146**, 308–325.

Paster T. P., Schauwecker D. S. and Haskin L. A. (1974) The behavior of some trace elements during solidification of the Skaergaard layered series. *Geochim. Cosmochim. Acta* **38**, 1549–1577.

Pedersen A. K. (1979) Basaltic glass with high-temperature equilibrated immiscible sulphide bodies with native iron from Disko, central West Greenland. *Contrib. Mineral. Petrol.* **69**, 397–407.

Pichavant M., Mysen B. and MacDonald R. (2002) Source and H_2O content of high-MgO magmas in island arc settings: an experimental study of a primitive calc-alkaline basalt from St. Vincent, lesser antilles arc. *Geochim. Cosmochim. Acta* **66**, 2193–2209.

Prouteau G. and Scaillet B. (2013) Experimental constraints on sulphur behaviour in subduction zones: implications for TTG and Adakite production and the global sulphur cycle since the Archean. *J. Petrol.* **54**, 183–213.

Richards J. P. (2009) Postsubduction porphyry Cu-Au and epithermal Au deposits: Products of remelting of subduction-modified lithosphere. *Geology* **37**, 247.

Richards J. P. (2011) High Sr/Y arc magmas and porphyry Cu ± Mo ± Au deposits: just add water. *Econ. Geol.* **106**, 1075–1081.

Ripley E. M. and Brophy J. G. (1995) Solubility of copper in a sulfur-free mafic melt. *Geochim. Cosmochim. Acta* **59**, 5027–5030.

Ripley E. M., Brophy J. G. and Li C. (2002) Copper solubility in a basaltic melt and sulfide liquid/silicate melt partition coefficients of Cu and Fe. *Geochim. Cosmochim. Acta* **66**, 2791–2800.

Scaillet B., Pichavant M., Roux J., Humbert G. and Lefevre A. (1992) Improvements of the Shaw membrane technique for measurement and control of f H2 at high temperatures and pressures. *Am. Mineral.* **77**, 647–655.

Shafiei B., Haschke M. and Shahabpour J. (2009) Recycling of orogenic arc crust triggers porphyry Cu mineralization in Kerman Cenozoic arc rocks, southeastern Iran. *Miner. Deposita* **44**, 265–283.

Simon A. C., Pettke T., Candela P. A., Piccoli P. M. and Heinrich C. A. (2006) Copper partitioning in a melt–vapor–brine–magnetite–pyrrhotite assemblage. *Geochim. Cosmochim. Acta* **70**, 5583–5600.

Simon A. C., Candela P. A., Piccoli P. M., Mengason M. and Englander L. (2008) The effect of crystal-melt partitioning on the budgets of Cu, Au, and Ag. *Am. Mineral.* **93**, 1437.

Sun C. and Liang Y. (2013) The importance of crystal chemistry on REE partitioning between mantle minerals (garnet, clinopyroxene, orthopyroxene, and olivine) and basaltic melts. *Chem. Geol.* **358**, 23–36.

Sun W., Zhang H., Ling M.-X., Ding X., Chung S.-L., Zhou J., Yang X.-Y. and Fan W. (2011) The genetic association of adakites and Cu–Au ore deposits. *Int. Geol. Rev.* **53**, 691–703.

Sun W. D., Liang H. Y., Ling M. X., Zhan M. Z., Ding X., Zhang H., Yang X. Y., Li Y. L., Ireland T. R., Wei Q. R. and Fan W. M. (2013) The link between reduced porphyry copper deposits and oxidized magmas. *Geochim. Cosmochim. Acta* **103**, 263–275.

Toplis M. (2005) The thermodynamics of iron and magnesium partitioning between olivine and liquid: criteria for assessing and predicting equilibrium in natural and experimental systems. *Contrib. Mineral. Petrol.* **149**, 22–39.

Ubide T., Galé C., Arranz E., Lago M. and Larrea P. (2014) Clinopyroxene and amphibole crystal populations in a lamprophyre sill from the Catalonian Coastal Ranges (NE Spain): a record of magma history and a window to mineral–melt partitioning. *Lithos* **184**, 225–242.

Walter M. J. (1998) Melting of garnet peridotite and the origin of komatiite and depleted lithosphere. *J. Petrol.* **39**, 29–60.

Wang Q., Xu J. F., Jian P., Bao Z. W., Zhao Z. H., Li C. F., Xiong X. L. and Ma J. L. (2006) Petrogenesis of adakitic porphyries in an extensional tectonic setting, Dexing, South China: implications for the genesis of porphyry copper mineralization. *J. Petrol.* **47**, 119.

Xiong X., Adam J. and Green T. (2005) Rutile stability and rutile/melt HFSE partitioning during partial melting of hydrous basalt: implications for TTG genesis. *Chem. Geol.* **218**, 339–359.

Yao L., Sun C. and Liang Y. (2012) A parameterized model for REE distribution between low-Ca pyroxene and basaltic melts with applications to REE partitioning in low-Ca pyroxene along a mantle adiabat and during pyroxenite-derived melt and peridotite interaction. *Contrib. Mineral. Petrol.* **164**, 261–280.

Yurimoto H. and Ohtani E. (1992) Element partitioning between majorite and liquid: a secondary ion mass spectrometric study. *Geophys. Res. Lett.* **19**, 17–20.

Zack T. and Brumm R. (1998) Ilmenite/liquid partition coefficients of 26 trace elements determined through ilmenite/clinopyroxene partitioning in garnet pyroxene. In *Proceedings of the 7th International Kimberlite Conference*. Red Roof Design, Cape Town.

Zajacz Z. and Halter W. (2007) LA-ICPMS analyses of silicate melt inclusions in co-precipitated minerals: quantification, data analysis and mineral/melt partitioning. *Geochim. Cosmochim. Acta* **71**, 1021–1040.

Zajacz Z., Seo J. H., Candela P. A., Piccoli P. M. and Tossell J. A. (2011) The solubility of copper in high-temperature magmatic vapors: a quest for the significance of various chloride and sulfide complexes. *Geochim. Cosmochim. Acta*.

Zajacz Z., Candela P. A., Piccoli P. M., Wälle M. and Sanchez-Valle C. (2012) Gold and copper in volatile saturated mafic to intermediate magmas: solubilities, partitioning, and implications for ore deposit formation. *Geochim. Cosmochim. Acta*.

Zajacz Z., Candela P. A., Piccoli P. M., Sanchez-Valle C. and Walle M. (2013) Solubility and partitioning behavior of Au, Cu, Ag and reduced S in magmas. *Geochim. Cosmochim. Acta* **112**, 288–304.

Associate editor: Edward M. Ripley